Crack growth behavior in plasma-sprayed thermal barrier coatings

Shijie Zhu[1], Zhaoxiang Chen[2] and Lihe Qian[2]

[1] Fukuoka Institute of Technology, Fukuoka, Japan

[2] Research Institute for Applied Mechanics, Kyushu University, Fukuoka, Japan

zhu@fit.ac.jp

ABSTRACT. *Ceramic thermal barrier coatings (TBCs) are increasingly applied to enhance the performance of advanced gas turbine engines. However, the delamination cracks initiated in these coatings limit their applications. In this research, a sandwiched four point bend specimen was used to evaluate the crack growth resistance in plasma sprayed TBCs. Well controlled, stable and measurable crack extension was obtained. A rising crack growth resistance curve was found. The steady state strain energy release rate was obtained to be ~ 170 J/m^2. The delamination crack evolution behavior was in-situ observed and simulated by finite element analysis based on a bridging model.*

INTRODUCTION

Crack growth resistance is an important mechanical property of plasma-sprayed thermal barrier coatings (TBCs) which usually fail due to spallation of the coatings from the substrate. Although there have been a number of research activities to establish a standard methodology for evaluating interfacial fracture toughness in TBCs, all of them are not satisfactory and the reported data on crack growth resistance in terms of interfacial strain energy release rate (G) or fracture toughness in plasma-sprayed TBCs vary largely. For example, the G values of air plasma sprayed (APS) Al_2O_3 coatings have been reported as 12 ~ 40 J/m^2 [1,2] and the values of APS ZrO_2-Y_2O_3 coatings vary between 25 ~ 200 J/m^2 [2-5]. The scatter in the measured toughness data primarily originates from the used test methods. It is known that the Vickers indentation technique [2-4], wedge opening load technique [6] and sandwiched three point bend specimen [7] have been attempted, but each of them is not applicable for long crack propagation. The sandwiched double cantilever beam (DCB) specimen has been used for long crack propagation in TBCs [1]. However, this technique needs a compliance calibration curve for crack length prediction, which is nonlinear and complicated [1]. Additionally, it is difficult to obtain a measurable, stable crack extension by using this specimen [1]. Recently, a sandwiched four point bend specimen was used, in which a complicated equation considering the specimen thickness was adopted for calculating strain energy release rate and finite element calculations of compliance were employed

for predicting crack lengths [8]. The questions are whether this method is applicable to TBCs and how to simplify it for application in engineering. Therefore, a more feasible and reasonable method needs to be developed in order to obtain reliable and reproducible interfacial fracture toughness in TBCs.

This paper reports an in-situ measurement of interfacial crack growth resistance in APS TBCs by using sandwiched four point bend specimen. The technique reported in this paper, compared to that in Ref. [8], is more convenient for thin ceramic films since the thickness of the thin film is ignored and its Young's modulus is not needed, accurate value of which is difficult to measure. Furthermore, crack lengths can be directly obtained from specimen side surface because crack growth is controllable, stable and measurable. Using this technique, the variation of strain energy release rate with crack length was measured and a rising R-curve was obtained. Finally, the delamination crack evolution behavior was in-situ observed for understanding the fracture mechanism in the APS TBCs.

EXPERIMENTAL PROCEDURES

A well-polished and cleaned SUS304 stainless steel plate of 5mm in thickness was used as the substrate material. A NiCoCrAlY alloy (Co23Cr17Al13Y0.5 and balance Ni) was used as the bond coat layer. The bond coat layer was deposited on the substrate using APS method. A partially stabilized ZrO_2 with 8 wt.%Y_2O_3 was used as the top coat layer and the top coat layer was deposited on the bond coat layer by APS method. The average thickness of either the bond coat or the top coat was ~150 μm.

Sandwiched four point bend specimen (Figure 1) was used for the experiment. The substrate of the as-deposited specimen was reduced to a thickness of about 3 mm. Then, a stiffener, which was made of the same material and with the same thickness as the substrate, was fixed to the surface of the top coat layer using a strong epoxy base adhesive. Hence, the coating layers were sandwiched between the substrate and the stiffener.

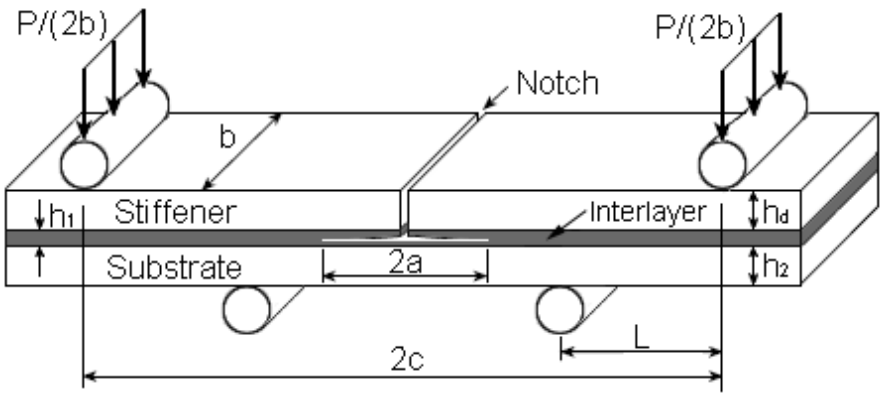

Figure 1. Geometry of sandwiched four point bend specimen (mm in unit).

The width and half length of the sandwiched specimen were ~ 7 and 25 mm, respectively. After preparing the sandwiched specimens, the side surfaces of the specimens were carefully polished up to 1 μm diamond paste finish. A notch was carefully cut through the stiffener and the adhesive layer, and into the top coat layer with a diamond saw such that the notch tip was laid within the top coat layer.

Pre-cracks were introduced from the notched specimens by fatigue on a servo-hydraulic test machine in an ambient air by using three point bend fixture with a span of 40 mm. The compression-compression load ratio was 0.1 and the frequency was 20 Hz for the fatigue pre-cracking. The pre-cracks initiated from the notch tips, then propagated and kinked symmetrically towards both sides of the notch, and finally entered into the plane close and parallel to the interface between the bond coat and top coat layers, as shown in Figure 2.

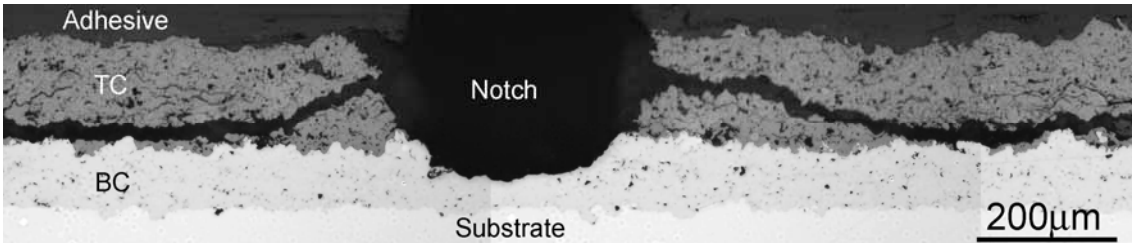

Figure 2. Typical crack path in the sandwiched TBCs sample after the bend test.

After pre-cracking, the specimens were monotonically loaded under four point bending at a constant loading rate of 2 N/s. The inner and outer spans of the four point bend fixture were 20 and 40 mm, respectively. The testing was performed in an ambient air using the same servo-hydraulic test machine as for fatigue pre-cracking. The load and crosshead displacement were continuously recorded using a digital recording system at a sampling rate of 100 ms. The crack length was directly measured from the polished surface during loading by means of a video camera and a traveling microscope. The crack length, a, was defined as a sum of the initial crack length, a_0, and the crack extension, Δa. The initial crack length, a_0, was determined as the distance from the notch root to the fatigue pre-crack tip, and the crack extension, Δa, was defined as the distance from the fatigue pre-crack tip to the crack front generated by monotonic loading. In the test, the specimen was unloaded after a crack extension of ~ 0.2 mm, and then reloaded to get another crack extension of ~ 0.2 mm. The loading-unloading process was repeated until the cracks on both sides were propagated to the inner loading lines.

A linear loading behavior was visible during the whole loading stage of the first cycle. No crack extension was detected after the first cycle. During the following each loading-unloading cycle, the initial linear loading behavior was followed by a non-linear behavior, which occurred near the maximum load on each curve and was accompanied by a crack extension. With increasing the number of loading-unloading cycles the applied maximum load was incremented, the crack length increased and the

slope of the linear portion in loading stage decreased. After complete unloading in each cycle, a permanent residual displacement appeared. The residual displacement was related to crack extension after each loading-unloading cycle.

Since sandwiched four point bend specimen was constructed by bonding a thin coating layer into two halves of substrate material, the whole bulk of the specimen was homogeneous except for the thin coating layer in the structure with a pre-existing crack lying close to the interface. According to Suo et al [9] strain energy release rate determined for homogeneous specimen with no layer can be used to characterize the interface crack in the presence of the layer by ignoring the layer when the thickness of the layer is small compared with the crack length and other in-plane scales of the specimen. In this way, the expressions of strain energy release rate for homogeneous DCB and compact tension (CT) specimens were used for sandwiched DCB and CT specimens to measure the interfacial fracture toughness of glass/Cu and Al_2O_3/Al interfaces [10,11]. Similarly, the expression for strain energy release rate of four point bend specimen with no sandwiched layer [12], G^{∞}, was adopted in this investigation to characterize the interfacial strain energy release rate in plasma-sprayed TBCs:

$$G^{\infty} = [21P^2L^2(1-\upsilon^2)]/16Eb^2h^3 \quad (1)$$

provided that the propagating interfacial cracks are located within the inner loading lines of the specimen, where P is the total load, L the spacing between the inner and outer loading lines, b and h the width and half height of the specimen, and E and υ the Young's modulus and Poisson's ratio of the substrate material.

RESULTS AND DISCUSSION

The cross sectional microstructures of the as-deposited coatings show that a lot of pores and curved inter-splat microcracks distribute uniformly in both the top coat and bond coat layers. In the bond coat layer, the curved microcracks are longer and sharper in the horizontal direction than in the vertical direction, whereas there is no such obvious difference in the top coat layer. The measurement of Raman spectra indicated that there are tetragonal phase and a small amount of monolithic phase of ZrO_2 in the top coat layer.

During testing, the crack evolution and propagation path were observed on one polished surface of the specimen using an optical microscope. It was found that the onset of the crack growth occurred from the initial fatigue pre-cracks. The delamination cracks on both sides of the notch were always extended within the top coat layer close and roughly parallel to the interface (Figure 3(a)). The entire cracks propagated within 10 ~ 60 μm from the interface. This crack trajectory is consistent with the failure mode most frequently observed in plasma sprayed TBCs [13,14]. This implies that the sandwiched four point bending technique is a feasible way to simulate the "in-service" delamination and evaluate strain energy release rate for the delamilation crack propagation in TBCs.

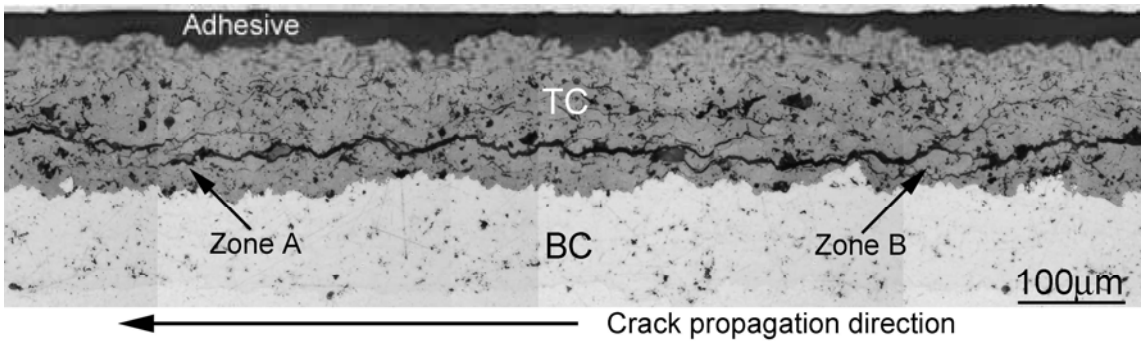

(a)

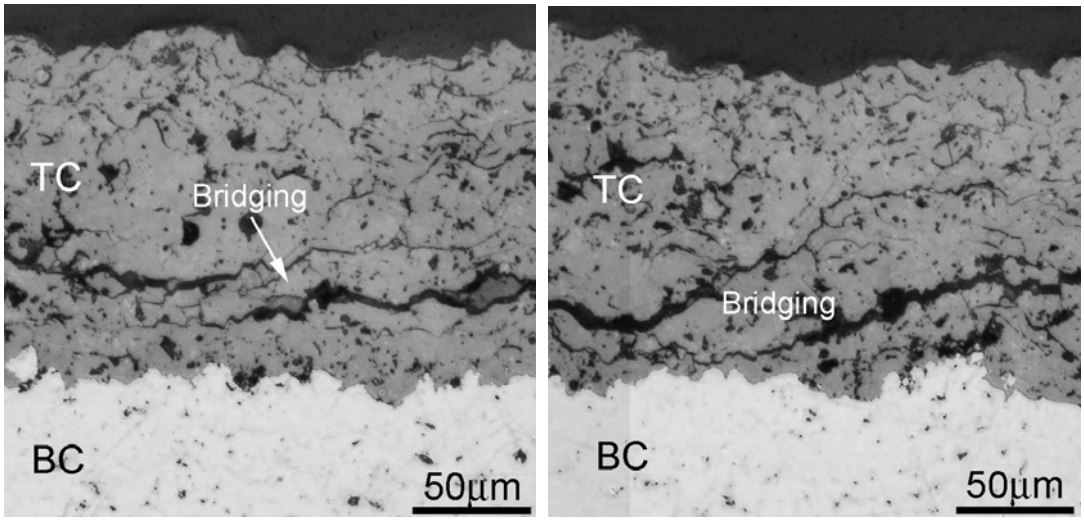

(b)

Figure 3. Crack morphology showing (a) crack propagation profile far behind the crack tip and (b) uncracked ligaments between two cracks.

Closer examination indicated that the delamination cracks propagated predominantly along inter-splat boundaries. Multiple, parallel short cracks were found in the crack tip region (Figure 3(b)). Between the overlapping parallel cracks were the uncracked ligaments, which bridged the parallel cracks. The crack bridging existed even in the wake zone far behind the main crack tip although it was more sparsely separated (Figure 3(a)).

The maximum load in each loading-unloading cycle was used to calculate the strain energy release rate at the corresponding crack length, a. The Young's modulus and Poisson's ratio of the substrate material were taken as 200 GPa and 0.3, respectively. A typical curve of the measured strain energy release rate, G^{∞}, as a function of crack extension, Δa, is shown in Figure 4. An obvious rising R-curve is visible. Multiple specimens for the measurement consistently demonstrated the same behavior.

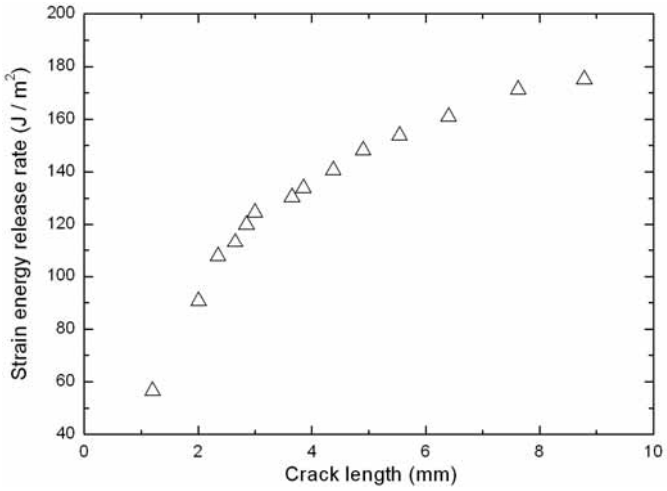

Figure 4. Measured strain energy release rate as a function of crack extension.

The R-curve starts at a value of ~ 100 J/m^2, increases rapidly over a crack growth distance of ~ 7 mm, and then gradually rises to a steady state value, G_{SS}^{∞}, ~ 170 J/m^2, at a crack length of ~ 9 mm. The steady state value of G_{SS}^{∞} obtained in this work is close to the strain energy release rate measured in Refs. [5] and [6] (150 ~ 200 J/m^2), but twice of the fracture work for delamination crack in Ref. [7] (71~81 J/m^2), and much higher than those measured in Refs. [2,3] (25 ~ 35 J/m^2) for APS ZrO_2-Y_2O_3 coatings. The difference in measured strain energy release rate could be caused by two factors: TBCs' microstructure and test method.

Although the tested materials were all composed of the standard composition (7 ~ 8 wt%YSZ), the coating process and spray parameters were different, which caused the variation in TBCs' microstructure. As fractographic observation indicated [15], there are many smooth surfaces and fresh rough surfaces on the fracture surface. The smooth surfaces are the faces of micropores, or inter-splat boundaries. The rough surfaces are formed as a result of discrete trans-lamellar microcracks between neighboring micropores or inter-splat boundaries. Macro-fracture occurs when sufficient micropores or inter-splat boundaries have been connected by trans-lamellar micropores to separate that region from the remainder of the coating. Therefore, the micropores or weak splat boundaries act as the crack initiation site and contribute to the major reductions in fracture resistance of TBCs, and thus the size, shape, orientation and size distribution of pores, and porosity level should be responsible for the difference in the reported fracture toughness.

It should also be argued that different test methods might generate different results. A notched specimen (2.6 × 4.6 × 3.5 mm^3) with a notch depth of 1.8 mm was used in wedge opening load technique in Ref. [6], and a pre-cracked specimen with a height of only 1.3 mm was used in three point bending approach in Ref. [7], where the crack was extended along the height direction. Clearly, cracks in their tests couldn't grow a sufficient distance to obtain potential R-curve behavior in TBCs.

The rising R-curve measured in the present research was attributed to the formation of bridging zone. In the wake zone behind the main crack tip existed many remaining regions, which have not been broken. The length of bridging zone increased with crack growth, and the bridging-caused toughening contribution enhanced accordingly. As a result, a rising R-curve formed. With a further increase in crack length, some unbroken ligaments began to fracture. Gradually, the bridging zone approached to a saturation state, and the size of this zone attained saturation. Thus, the toughness reached its steady state value. The finite element analysis was conducted using a bridging model as shown in Figure 5. The width (L) and number of the bridging ligaments were changed during crack growth simulation. The simulated results are shown in Figure 6 (triangles). It can be seen that the predicted results agree with experimental results (Figure 4). Without the bridging ligament, energy release rate does not increase with crack extension, as indicated by the circles.

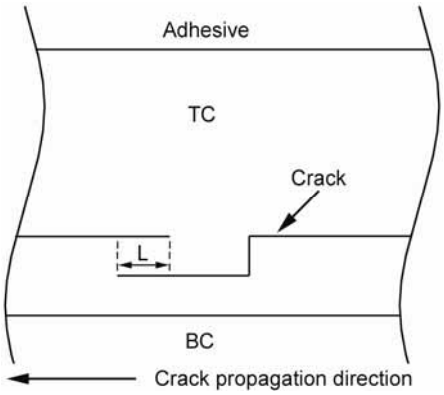

Figure 5. Crack bridging model for finite element analysis.

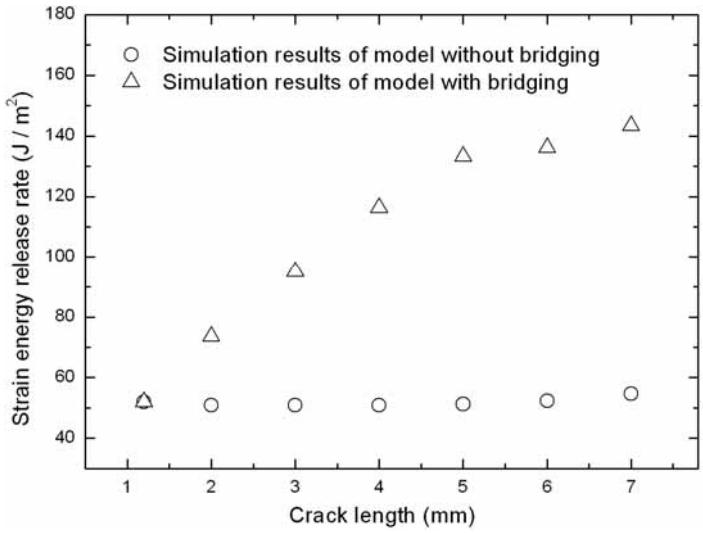

Figure 6. Simulated strain energy release rate as a function of crack extension.

CONCLUSION

The interfacial crack growth resistance in APS ZrO_2-8wt.%Y_2O_3 TBCs has been studied using sandwiched four point bend specimen. Delamination cracks were always propagated in the top coat layer but tended to approach to the interface between the bond coat and top coat layers. The strain energy release rate was measured to increase with crack extension, showing an obvious rising R-curve behavior. The rising R-curve in the APS TBCs was caused by the crack bridging in the wake zone, which shielded the crack tip from far-field loading.

REFERENCES

1. P. Ostojic, R. McPherson, J. Am. Ceram. Soc., 71, 891 (1988).
2. A. Rabiei and A.G. Evans, Acta Mater., 48, 3963 (2000).
3. A.H. Bartlett and R.D. Maschio, J.Am.Ceram. Soc. 78, 1018 (1995).
4. D.Z.Guo, L.J.Wang, Surf. Coat. Technol. 56, 19 (1992).
5. G.N. Heintze and R. McPherson, Surf. Coat. Technol., 34, 15 (1988).
6. E. Wessel and R.W. Steinbrech, Key Eng. Mater. 223, 55 (2002).
7. G. Thurn, G.A. Schneider, H.A. Bahr and F. Aldinger, Surf. Coat. Technol. 123, 147 (2000).
8. I. Hofinger, M. Oechsner, H-A. Bahr and M. V. Swain, Int. J. Fract., 92, 213 (1998).
9. Z. Suo, J.W. Hutchinson, Mater. Sci. Eng. A. 107, 135 (1989).
10. R.M. Cannon, B.J. Dalgleish, R.H. Dauskardt, T.S. Oh and R.O. Ritchie, Acta Metall. Mater., 39, 2145 (1991).
11. J.M. McNaney R.M. Cannon, and R.O. Ritchie, Acta Mater., 44, 4713 (1996)
12. P.G. Charalambides, J.Lund, A.G. Evans and R.M. McMeeking, J. App. Mech., Trans. ASME 56, 77 (1989).
13. R.A. Miller, J. Thermal Spray Tech. 6, 35 (1997).
14. S. Bose and J. DeMasi-Marcin, J. Thermal Spray Tech., 6, 99 (1997).
15. P.J. Callus and C.C. Berndt, Surf. Coat. Technol., 114, 114 (1999).